Supporting Information

Immiscible alloys as high-capacity and ultra-stable anodes for sodium-ion batteries

Xiaoying Zhao,‡[a] Ningbo Liu,‡[a] Liubin Wang,*[a] Xiaohan Wang,[a] Bin Qin,[b] Qiaqia Li,[a] Yinuo Xu,[a] Jing Liu[a] and Fujun Li*[c]

[a] College of Chemistry and Materials Science, Key Laboratory of Analytical Science and Technology of Hebei Province, Hebei Research Center of the Basic Discipline of Synthetic Chemistry, Hebei University, Baoding, Hebei 071002, China. E-mail: lbwang@hbu.edu.cn (L. Wang).

[b] Department of Chemistry, The University of Hong Kong, Pokfulam Road, Hong Kong SAR, China

[c] State Key Laboratory of Advanced Chemical Power Sources, Key Laboratory of Advanced Energy Materials Chemistry (Ministry of Education), College of Chemistry, Nankai University, Tianjin 300071, China. E-mail: fujunli@nankai.edu.cn (F. Li).

Contents

21. **Figure S21:** Compaision of the diffusion coefficients (D_{Na+}) of the PBS and P/B/S electrodes.

22. **Figure S22:** EIS spectra at different charge/discharge states of the P/B/S electrode.

23. **Figure S23:** Comparision of the rate performance in PBS and P/B/S electrodes.

24. **Figure S24:** SEM images of the PBS electrodes in the $NaClO_4$/PC/FEC.

25. **Figure S25:** Statistical diagram of the volume expansion ratio of the initial two cycles of the PBS alloy particles in Movie S1.

26. **Figure S26:** EDX mappings of the PBS electrode at different states.

27. **Figure S27:** XRD patterns of PBS electrode before and after 10000 cycles.

28. **Figure S28:** N_2 sorption/desorption isotherm and pore size distribution curves of PBS electrode before and after 100 cycles.

29. **Figure S29:** XPS spectra of different state electrodes in the $NaClO_4$-PC electrolyte.

30. **Figure S30:** HRTEM images of SEI film on the surface of charged PBS electrode.

31. **Figure S31:** Structure characterization and performance of $Na_3V_2(PO_4)_2F_3$.

32. **Figure S32:** CV curves of the NVPF//PBS full cell.

33. **Figure S33:** GCD curves at different current densities of the NVPF//PBS full cell.

34. **Figure S34:** Voltage, capacity, and energy density of several typical alloying-type anode based full SIBs.

35. **Table S1:** Melting point, phase composition, theoretical and experimental specific capacity of the as-prepared PBS alloys.

36. **Table S2:** Comparison of electrochemical performance of the PBS electrode with reported alloy anodes in SIBs.

37. **Table S3:** Fitted impendence parameters of the PBS and P/B/S electrodes at different charge/discharge states.

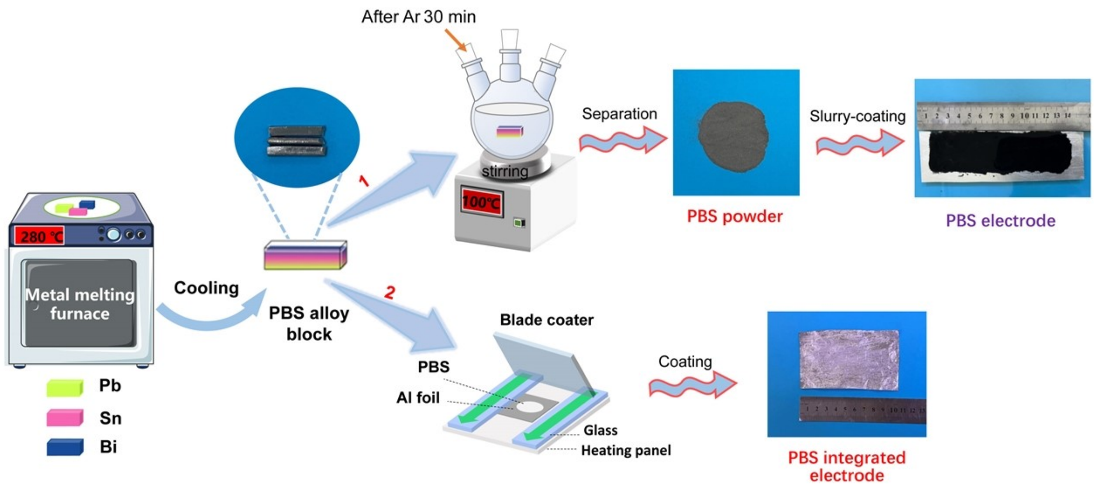

Figure S1. Schematic illustration of the synthesis steps of PBS electrode.

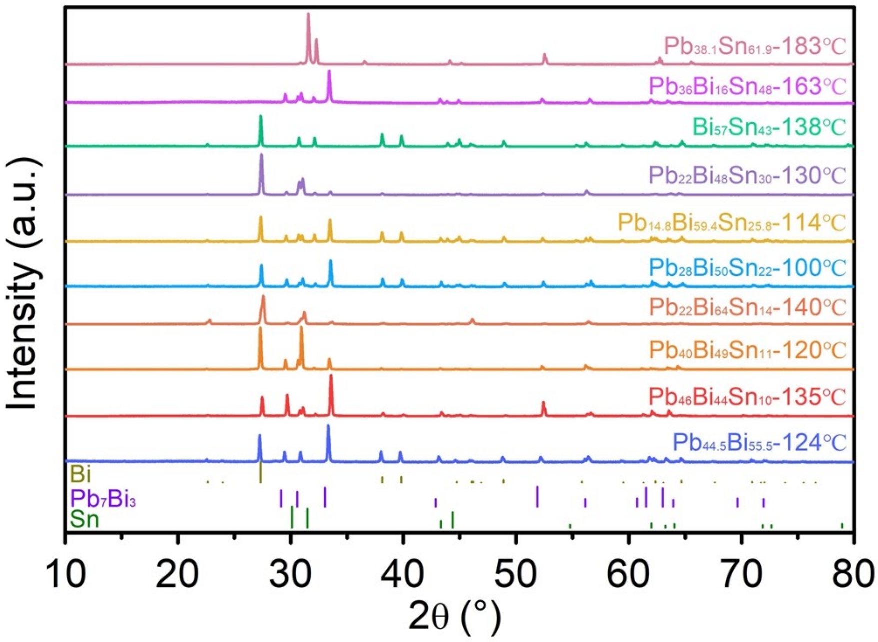

Figure S2. XRD patterns of PBS alloys with different proportions.

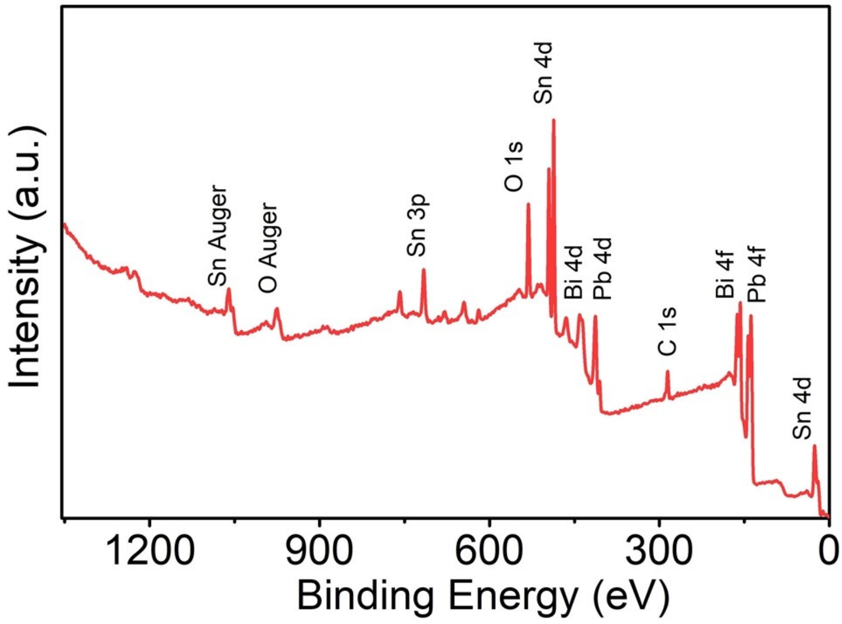

Figure S3. Full XPS survey spectrum of the $Pb_{32}Bi_{52.5}Sn_{15.5}$ alloy.

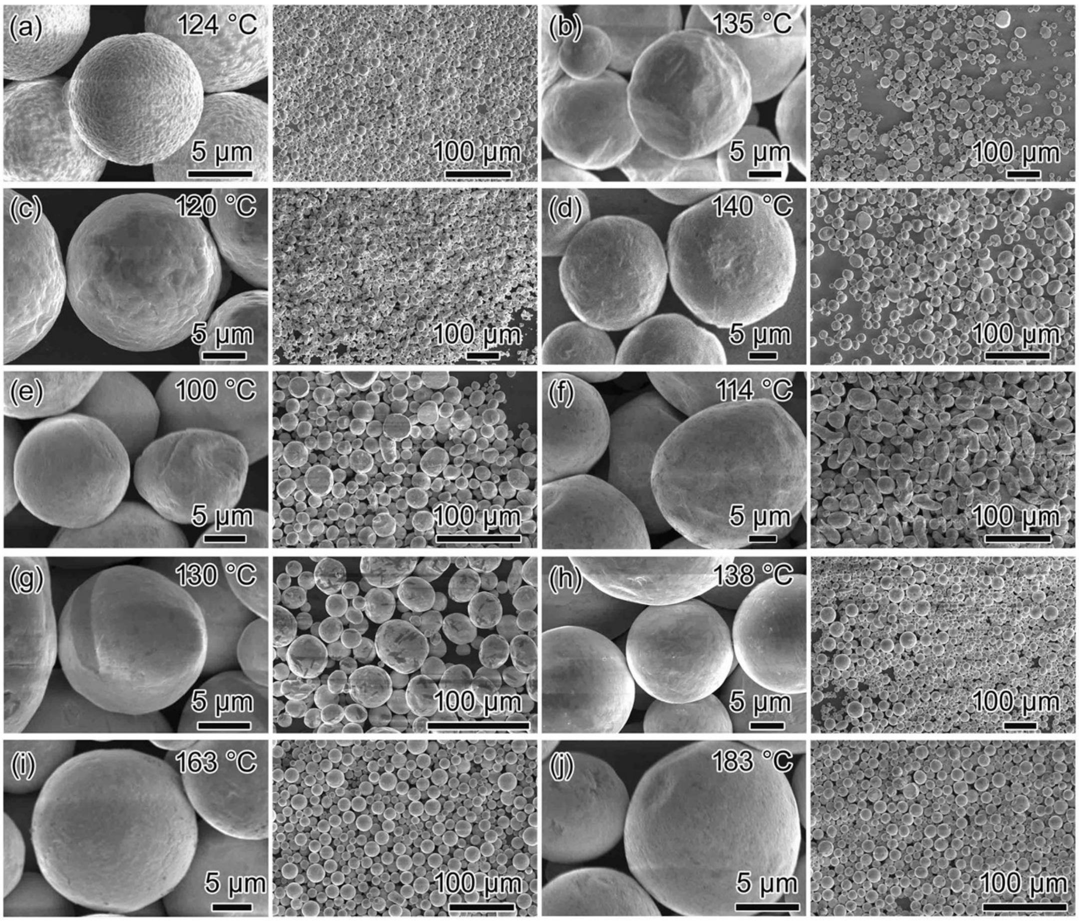

Figure S4. SEM images of the PBS powders synthesised with different proportions.

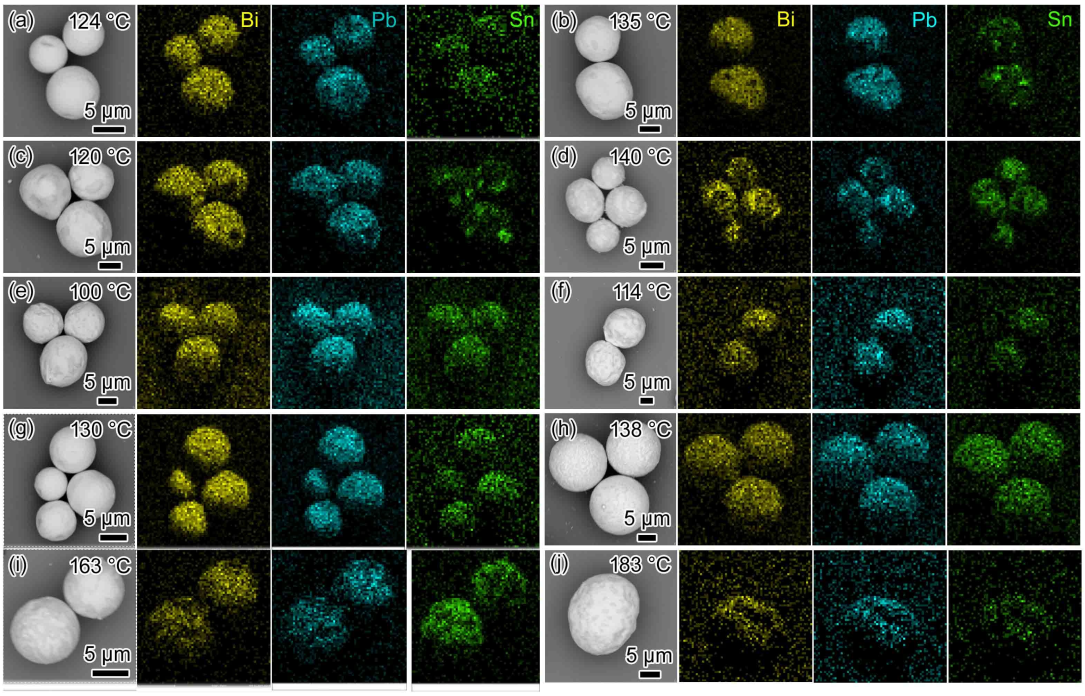

Figure S5. EDX elemental mapping images of the PBS alloys.

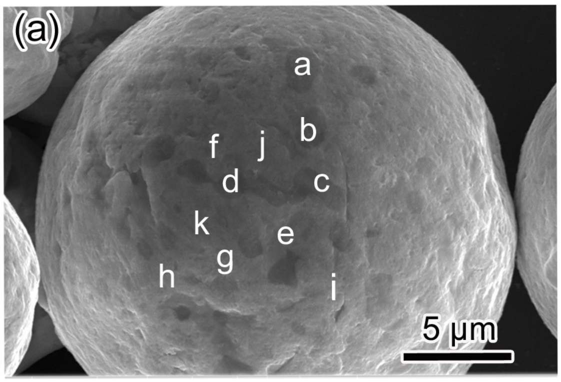

(b)	Pb (%)	Bi (%)	Sn (%)
a	1.64	6.69	91.67
b	5.54	5.81	88.65
c	5.08	9.51	85.41
d	6.45	8.29	85.26
e	48.88	42.05	9.07
f	44.63	52.00	3.37
g	41.75	41.85	16.40
h	13.66	64.63	21.71
i	21.36	56.81	21.83
j	45.07	41.36	13.57
k	51.76	39.29	8.95

Figure S6. SEM image of the $Pb_{32}Bi_{52.5}Sn_{15.5}$ alloy microsphere and corresponding component analysis with spot scan in EDX (Atomic percentage).

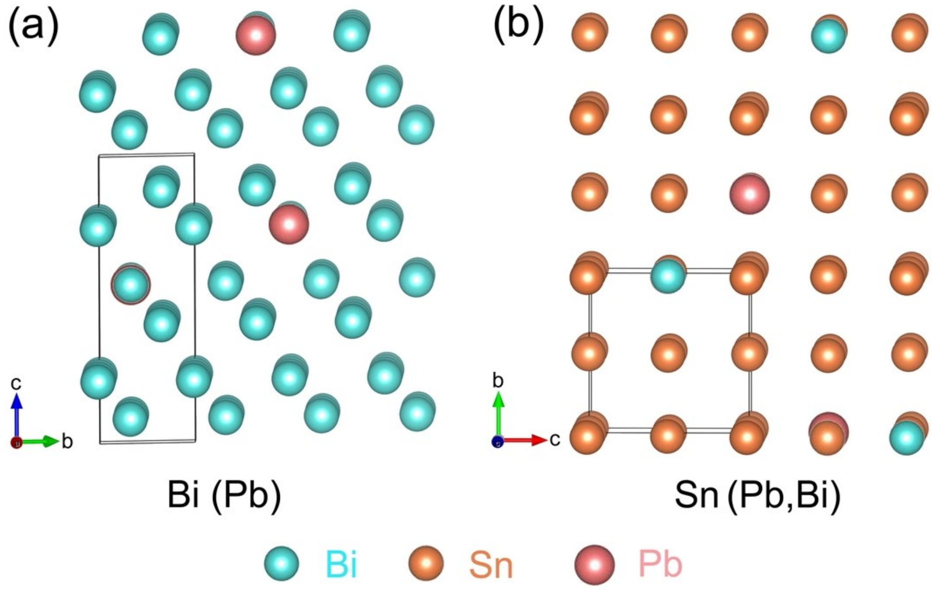

Figure S7. Crystal structure diagram of the solid solution in Bi-(Pb) and Sn-(Bi,Pb).

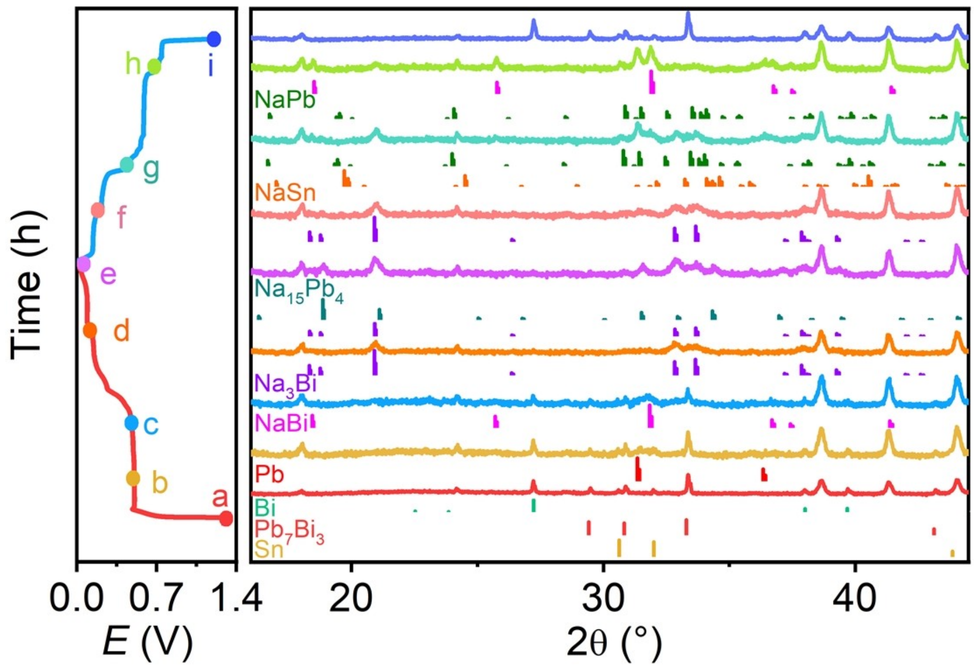

Figure S8. Selected *in-situ* XRD patterns of the PBS eletrode during the first cycle.

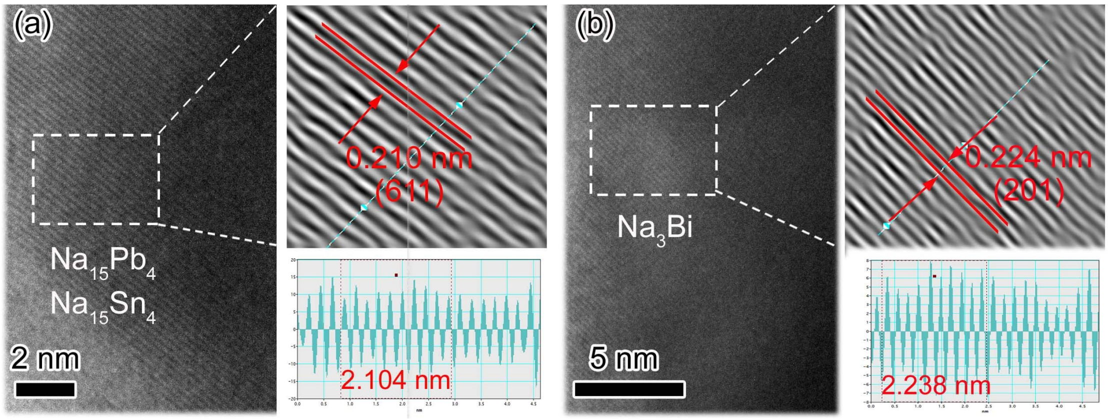

Figure S9. HRTEM images of the PBS electrode after discharged to 0.01 V.

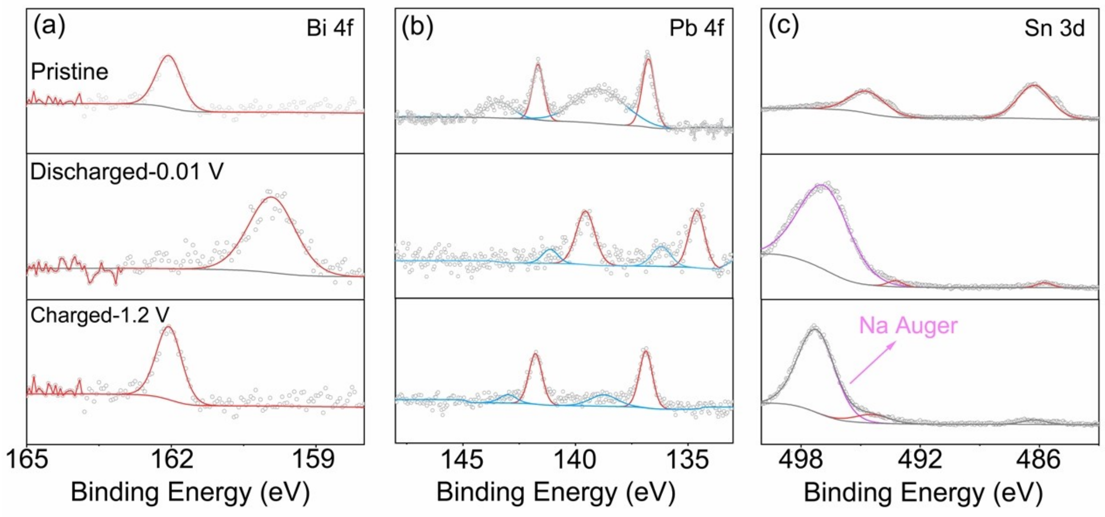

Figure S10. XPS spectra of Pb 4f, Sn 3d and Bi 4f of the pristine, discharged to 0.01 V and charged to 1.2 V state electrodes.

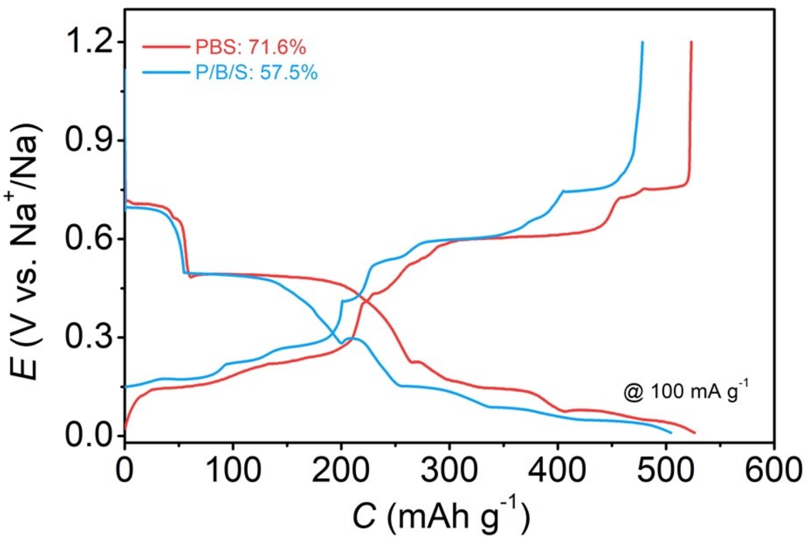

Figure S11. Comparision of the GCD curves of the PBS and P/B/S electrodes and the correspoding energy efficiency.

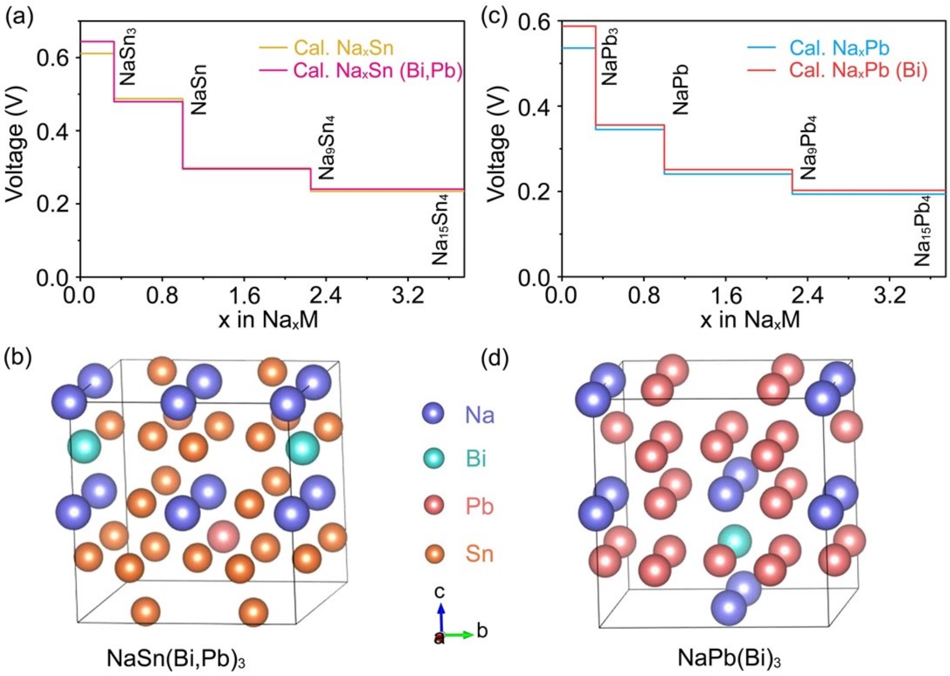

Figure S12. Calculated electrode potential profiles for the solid solution and pure phases and the corresponding schematic diagram of the solid solution structures.

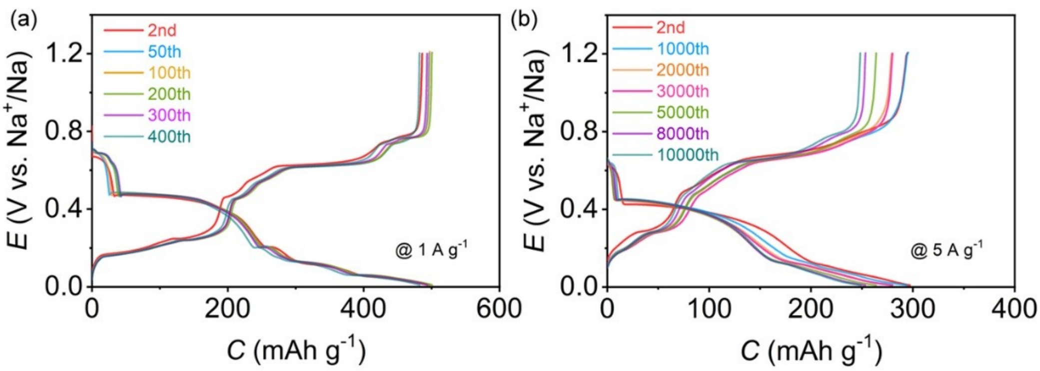

Figure S13. Discharge/charge curves of the PBS electrode with diffferent cycles at (a) 1 A g^{-1} and (b) 5 A g^{-1}.

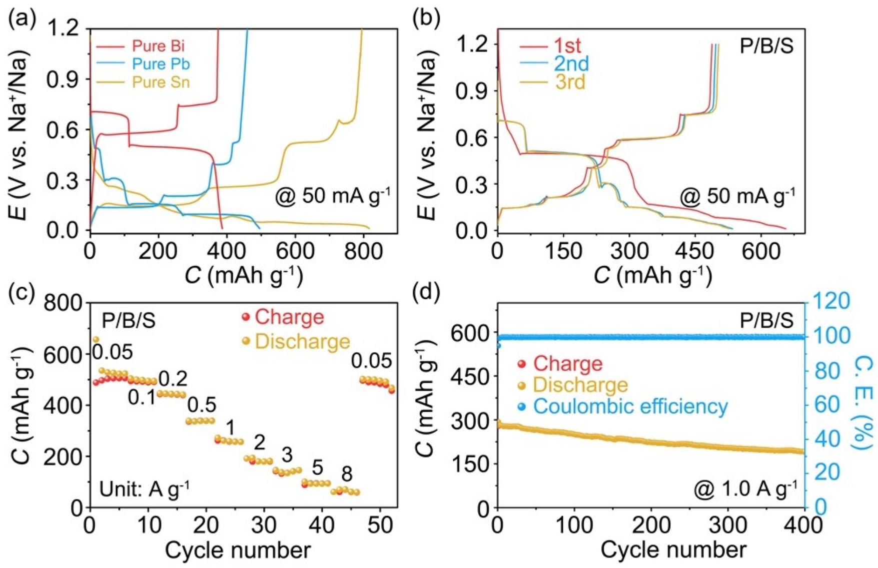

Figure S14. Electrochemical performance of pure Pb/Bi/Sn and P/B/S electrodes: a) GCD curves of the pure Pb/Bi/Sn electrodes; b) GCD curves at 50 mA g^{-1}; c) rate performance at 0.05 to 8.0 A g^{-1} and d) cycling performance at 1 A g^{-1} of the P/B/S electrode.

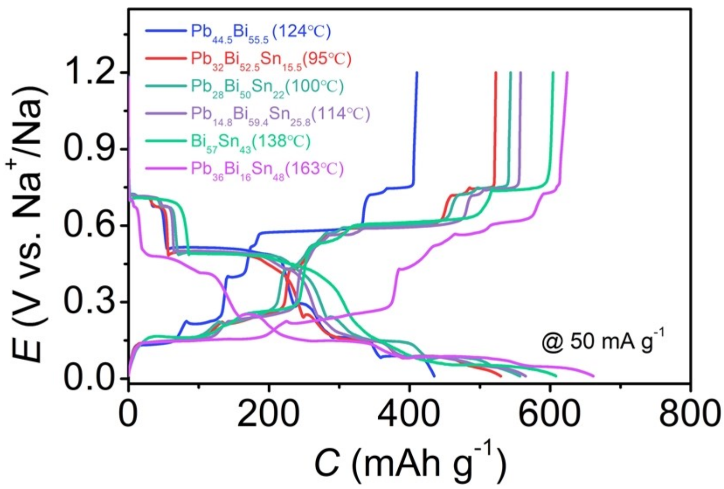

Figure S15. GCD curves of the other immiscible alloy electrodes.

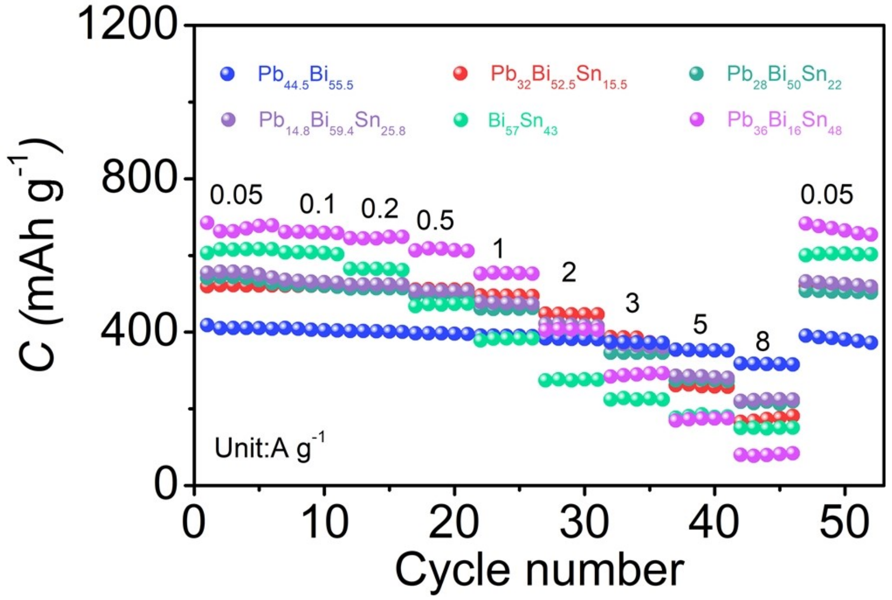

Figure S16. Comparision of rate performance of the immiscible alloy electrodes.

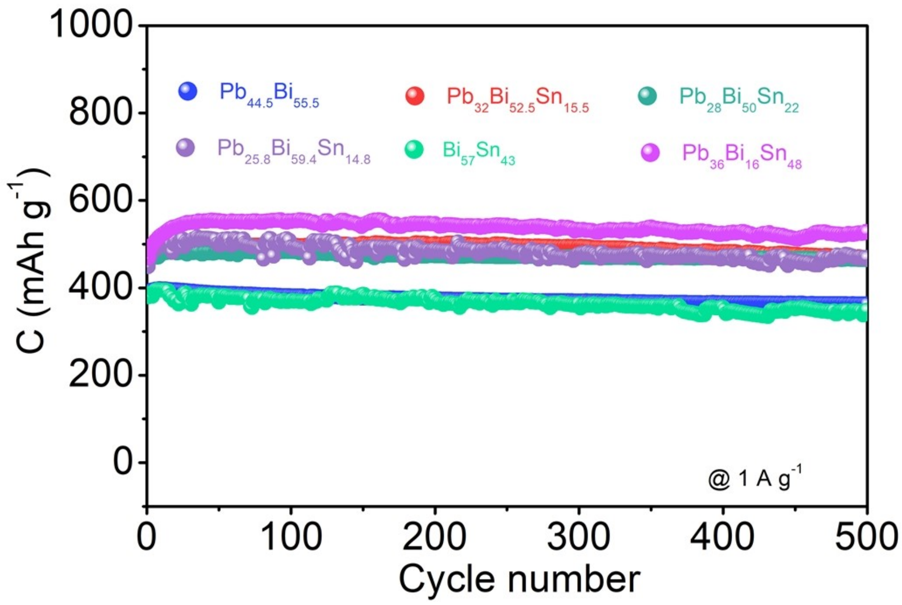

Figure S17. Cycling performance of the other immiscible alloy electrodes at 1 A g^{-1}.

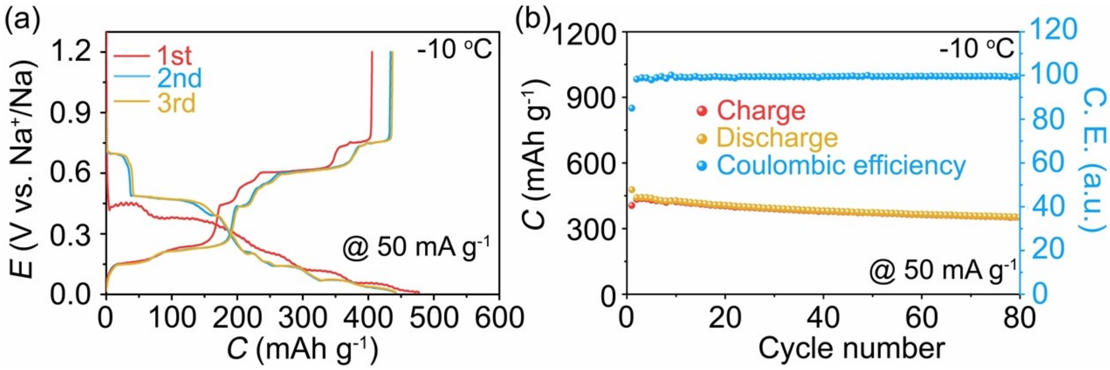

Figure S18. GCD curves and cycling performance of the PBS electrode at 50 mA g^{-1} test at a low temperature of -10 ^{o}C.

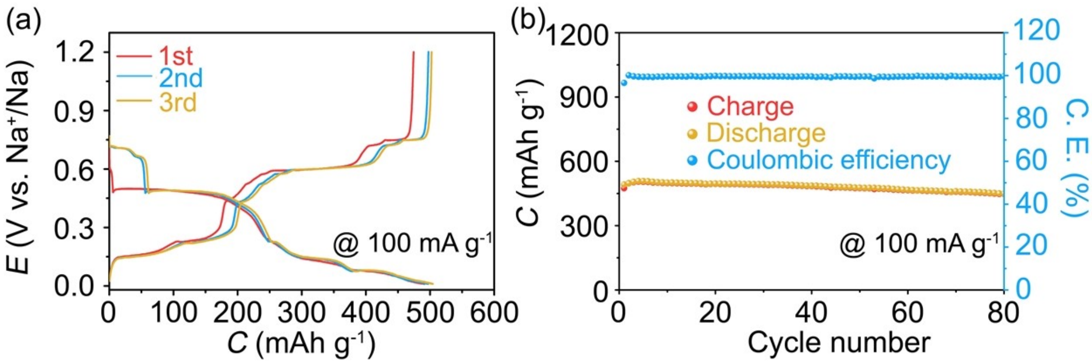

Figure S19. GCD curves and cycling performance of the integrated PBS electrode at 100 mA g^{-1}.

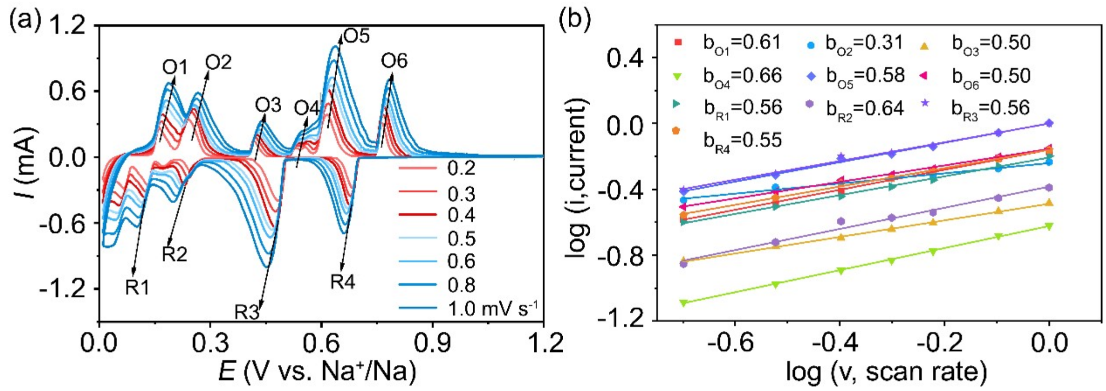

Figure S20. a) CV curves at different scan rates and b) the corresponding log*i* vs. log*v* plots for different redox peaks of the P/B/S eletrode.

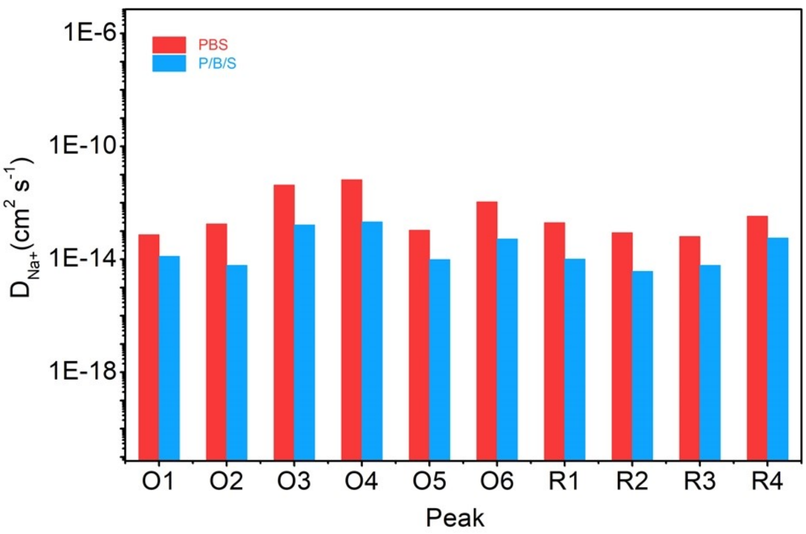

Figure S21. Compaision of the diffusion coefficients (D_{Na+}) of the PBS and P/B/S electrodes based on the Randles-Sevcik equation.

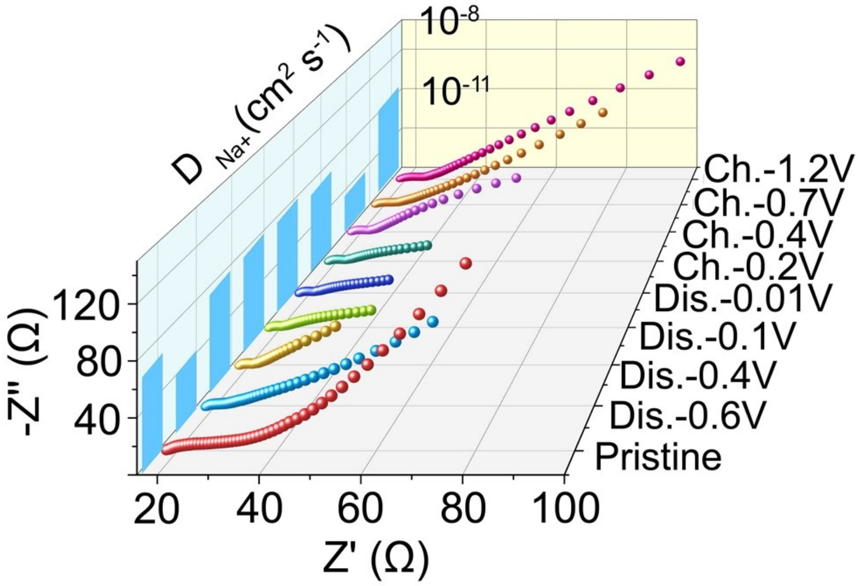

Figure S22. EIS spectra at different charge/discharge states of the P/B/S electrode and the corresponding calculated diffusion coefficients.

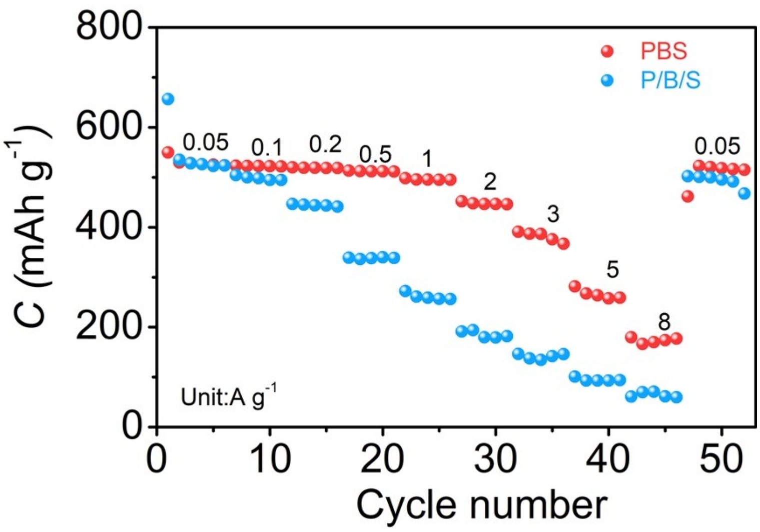

Figure S23. Comparision of the rate performance in PBS and P/B/S electrodes.

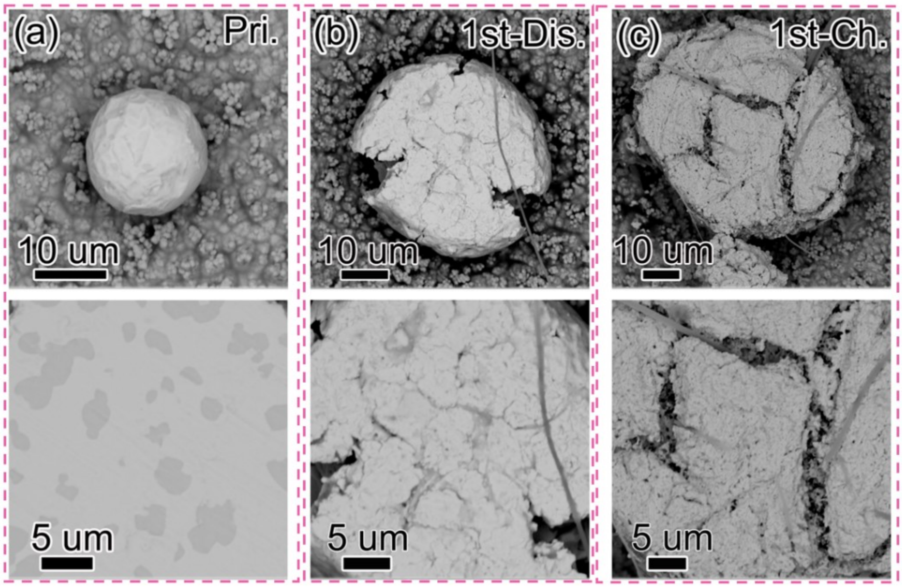

Figure S24. SEM images of the PBS electrodes before and after different cycles (1st-Dis., 1st-Ch.) in the $NaClO_4$/PC/FEC.

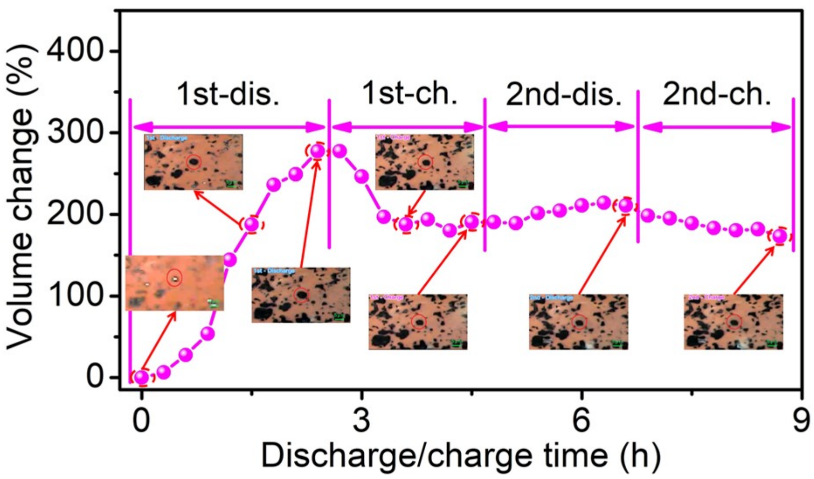

Figure S25. Statistical diagram of the volume expansion ratio of the initial two cycles of the PBS alloy particles in Movie S1.

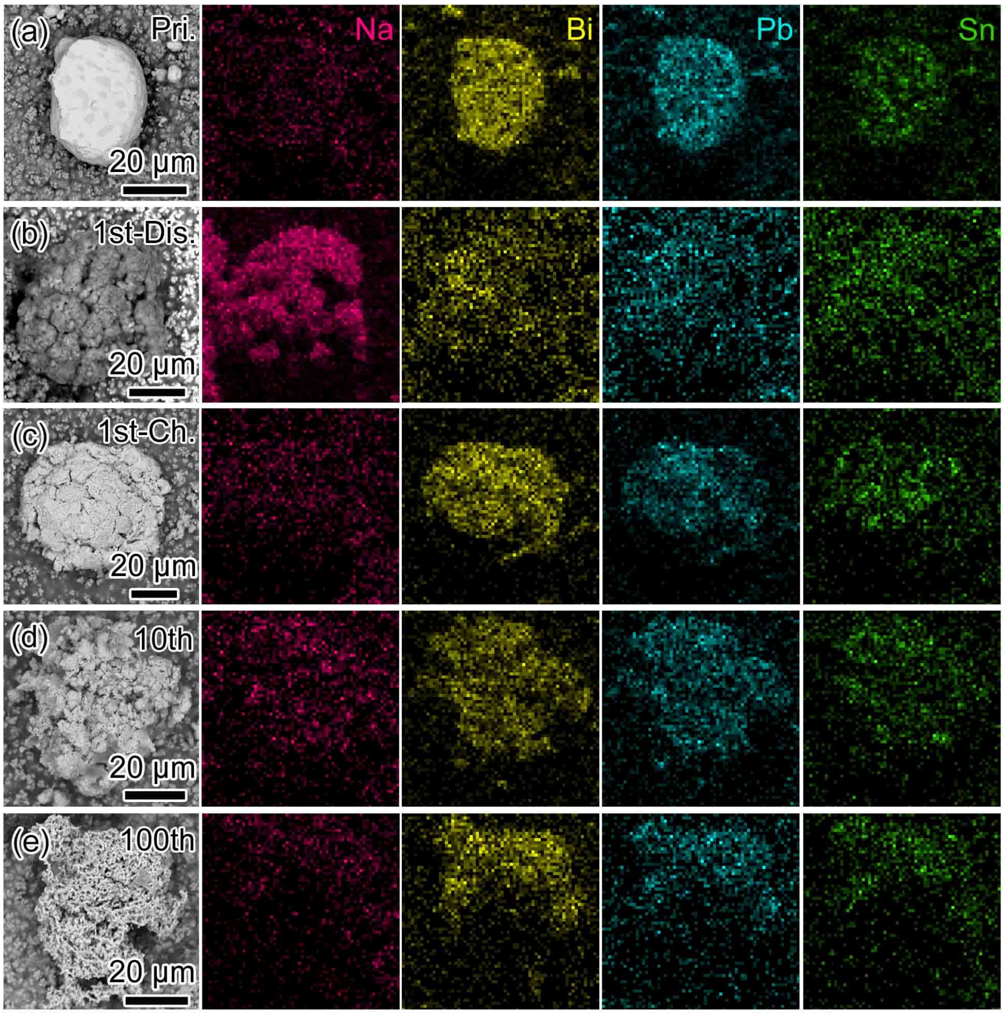

Figure S26. EDX mappings of the PBS electrode at different states: Pristine, 1st-Dis., 1st-Ch., 10th cycle, 100th cycle in the $NaPF_6$/DEGDME electrolyte, respectively.

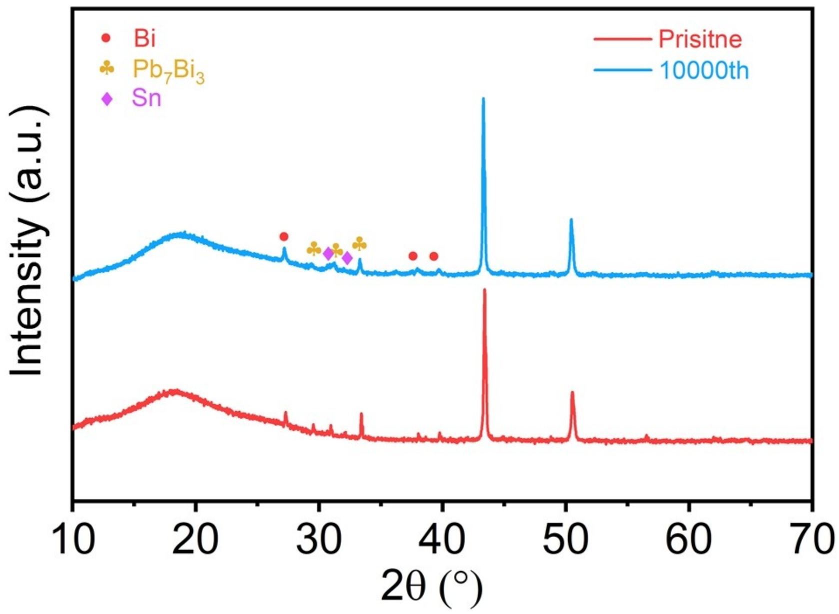

Figure S27. XRD patterns of PBS electrode before and after 10000 cycles.

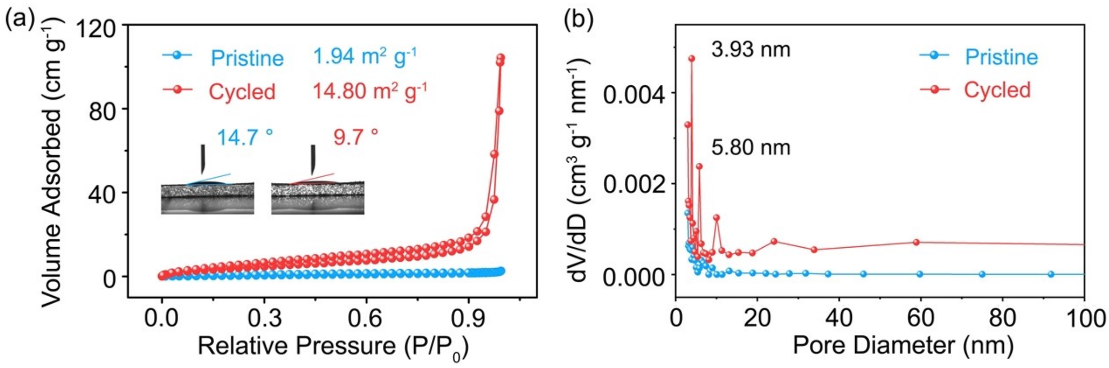

Figure S28. N_2 sorption/desorption isotherm and pore size distribution curves of PBS electrode before and after 100 cycles.

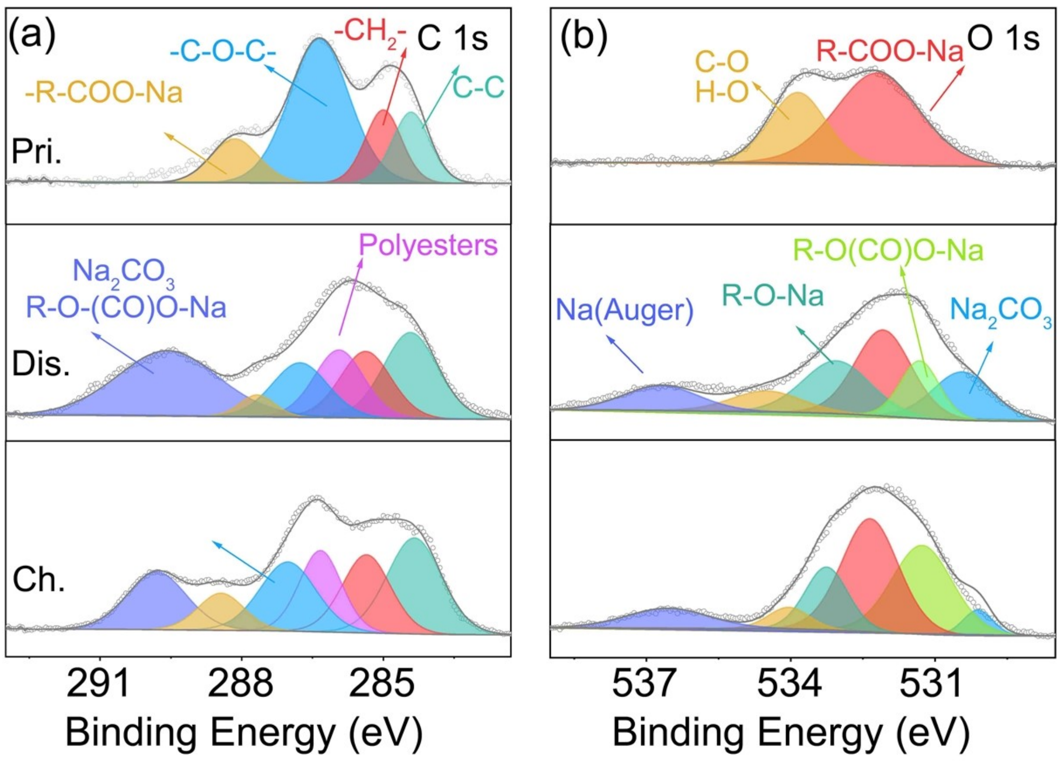

Figure S29. C 1s and O 1s XPS spectra of the pristine, discharged, and charged PBS electrodes in the $NaClO_4$-PC electrolyte.

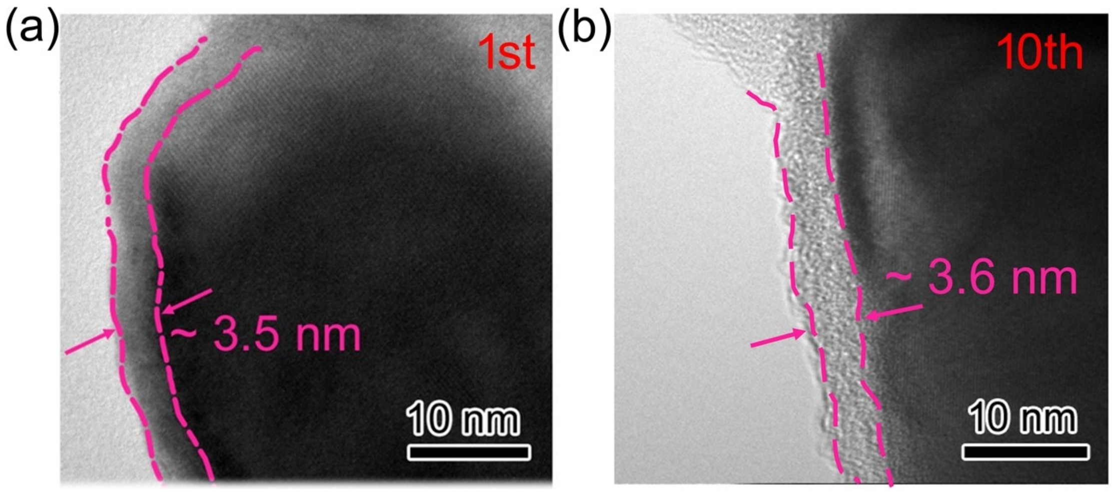

Figure S30. HRTEM images of SEI film on the surface of charged PBS electrode at the first and tenth cycle.

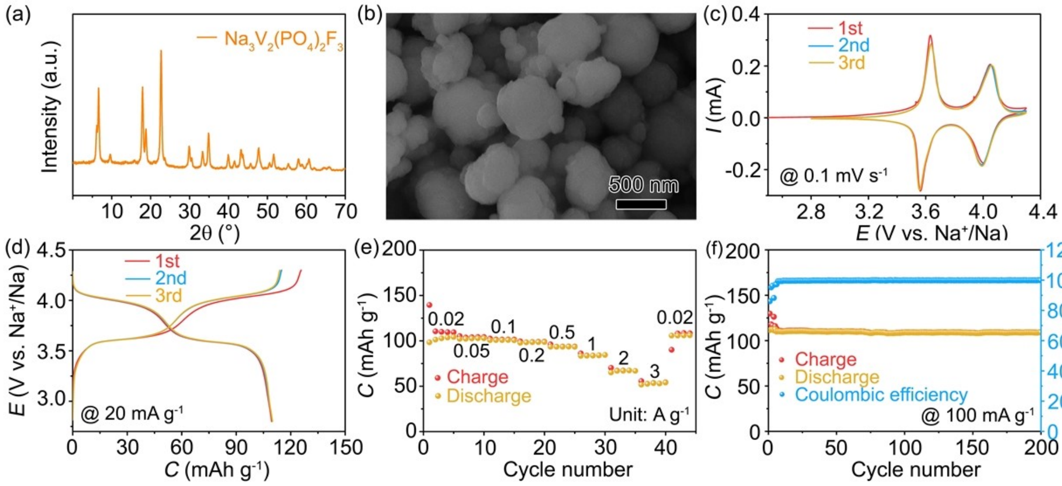

Figure S31. Structure characterization and performance of $Na_3V_2(PO_4)_2F_3$: a) XRD pattern; b) SEM image; c) CV curves at a scan rate of 0.1 mV s^{-1}; d) GCD curves at 20 mA g^{-1}; e) rate performance; f) cycling performance 100 mA g^{-1}.

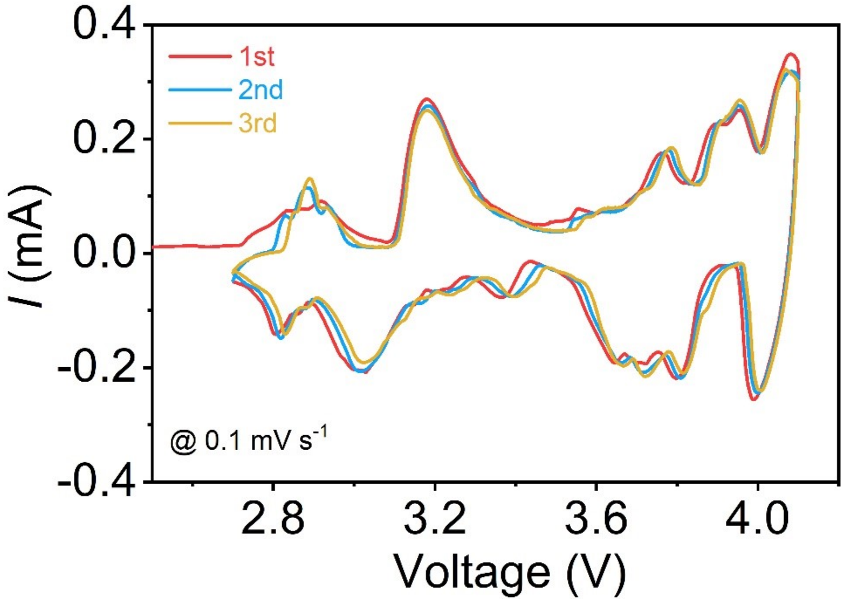

Figure S32. CV curves of the NVPF//PBS full cell at 0.1 mV s^{-1}.

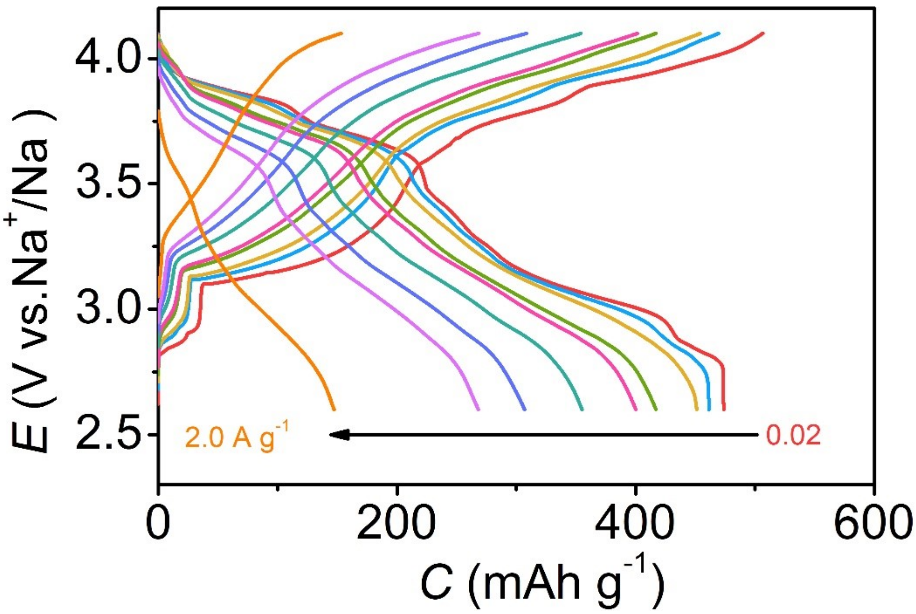

Figure S33. GCD curves at different current densities of the NVPF//PBS full cell.

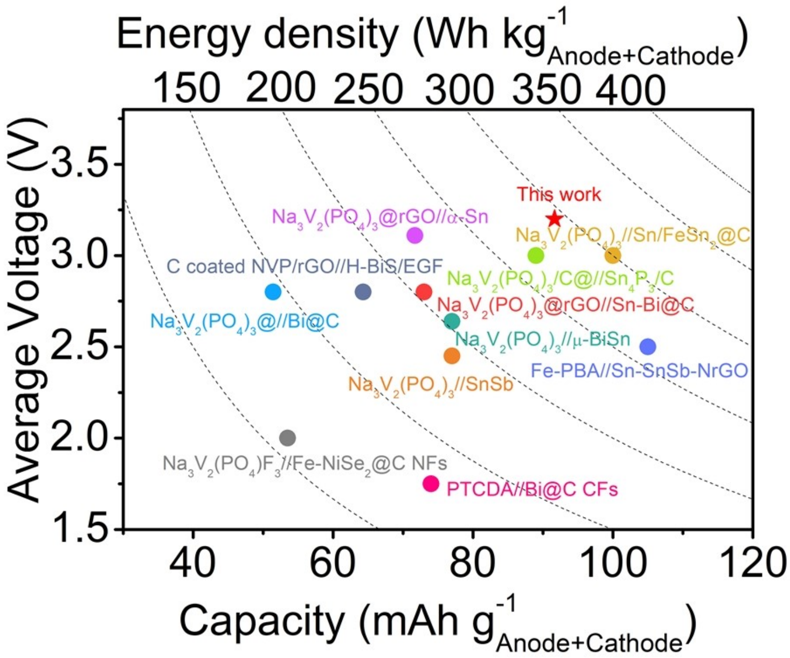

Figure S34. Voltage, capacity, and energy density of several typical alloying-type anode based full SIBs.

Table S1. Melting point, phase composition, theoretical and experimental specific capacity of the as-prepared PBS alloys.

Sample-wt%	Melting point (°C)	Phase composition	Theoretical specific capacity (mAh g^{-1})	Experimental specific capacity (mAh g^{-1})
$Pb_{44.5}Bi_{55.5}$	124	Pb_7Bi_3-Bi	429.53	425.99
$Pb_{46}Bi_{44}Sn_{10}$	135	Pb_7Bi_3-Bi-Sn	501.75	495.89
$Pb_{40}Bi_{49}Sn_{11}$	120	Pb_7Bi_3-Bi-Sn	504.97	500.92
$Pb_{22}Bi_{64}Sn_{14}$	140	Pb_7Bi_3-Bi-Sn	506.40	501.50
$Pb_{32}Bi_{52.5}Sn_{15.5}$	95	Pb_7Bi_3-Bi-Sn	526.31	526.04
$Pb_{28}Bi_{50}Sn_{22}$	100	Pb_7Bi_3-Bi-Sn	561.89	556.73
$Pb_{14.8}Bi_{59.4}Sn_{25.8}$	114	Pb_7Bi_3-Bi-Sn	572.33	568.30
$Pb_{22}Bi_{48}Sn_{30}$	130	Pb_7Bi_3-Bi-Sn	601.41	588.60
$Bi_{57}Sn_{43}$	138	Bi-Sn	648.04	606.70
$Pb_{36}Bi_{16}Sn_{48}$	163	Pb_7Bi_3-Sn	696.80	663.40
$Pb_{38.1}Sn_{61.9}$	183	Pb-Sn	752.30	700.39

Table S2. Comparison of electrochemical performance of the PBS electrode with reported alloy anodes in SIBs.

Sample	Initial Coulombic efficiency	Reversible Capacity	Cycling performance	Rate performance	Reference
PBS	95%	523 mAh g^{-1} @0.05 A g^{-1}	87% (10000 cycles) 5 A g^{-1}	264 mAh g^{-1} @5 A g^{-1}	This work
Pb	58%	381 mAh g^{-1} @4.8 A g^{-1}	64% (1000 cycles) @4.8 A g^{-1}	200 mAh g^{-1} @12 A g^{-1}	1
Sb/C/NS	68%	410 mAh g^{-1} @0.1 A g^{-1}	88% (100 cycles) @0.1 A g^{-1}	324 mAh g^{-1} @10 A g^{-1}	2
Sn@NC	78%	507 mAh g^{-1} @0.1 A g^{-1}	82% (400 cycles) @0.1 A g^{-1}	437 mAh g^{-1} @5 A g^{-1}	3
Bi@C	57%	919 mAh g^{-1} @0.1 A g^{-1}	38% (80 cycles) @0.1 A g^{-1}	175 mAh g^{-1} @1.6 A g^{-1}	4
Bi NTs	69%	401 mAh g^{-1} @0.1 A g^{-1}	77% (5000 cycles) @1 A g^{-1}	350 mAh g^{-1} @150 A g^{-1}	5
SbSn	81%	650 mAh g^{-1} @0.2 A g^{-1}	88% (200 cycles) @1.5A g^{-1}	521 mAh g^{-1} @3.7A g^{-1}	6
Sn	80%	620 mAh g^{-1} @0.1 A g^{-1}	80% (3500 cycles) @2 A g^{-1}	464 mAh g^{-1} @4 A g^{-1}	7
SnBi@C	80%	610 mAh g^{-1} @0.1 A g^{-1}	99% (4500 cycles) @5 A g^{-1}	372 mAh g^{-1} @10 A g^{-1}	8
$Bi_{0.7}Sb_{0.3}$	72%	520 mAh g^{-1} @200 mA g^{-1}	71% (50 cycles) @0.2 A g^{-1}	285 mAh g^{-1} @2 A g^{-1}	9
FBi@NC	73%	433 mAh g^{-1} @1 A g^{-1}	82% (8000 cycles) @10 A g^{-1}	368 mAh g^{-1} @30 A g^{-1}	10
np-Bi_2Sb_6	61%	455 mAh g @0.2 A g^{-1}	37% (2000 cycles) @0.2 A g^{-1}	304 mAh g^{-1} @15 A g^{-1}	11
Sb/C	55%	440 mAh g^{-1} @0.1 A g^{-1}	75% (300 cycles) @0.1 A g^{-1}	88 mAh g^{-1} @6 A g^{-1}	12
Sn@CFC	42%	300 mAh g^{-1} @0.05 A g^{-1}	80% (1000 cycles) @0.2 A g^{-1}	170 mAh g^{-1} @0.5 A g^{-1}	13

Table S3. Fitted impendence parameters of the PBS and P/B/S electrodes at different charge/discharge states.

State	Rct (Ω)		Rs (Ω)	
	PBS	P/B/S	PBS	P/B/S
Pristine	23.34	25.81	18.36	15.61
Dis.-0.6 V	15.54	18.38	5.6	3.70
Dis.-0.4 V	15.32	18.16	6.26	2.52
Dis.-0.1 V	15.08	17.55	5.93	2.81
Dis.-0.01 V	14.99	17.58	6.34	3.42
Ch.-0.2 V	16.18	17.96	5.43	4.28
Ch.-0.4 V	15.78	17.3	5.75	4.78
Ch.-0.7 V	15.29	17.87	8.98	6.94
Ch.-1.2 V	14.91	18.76	5.32	7.62

Reference

1. C. Kim, H. Kim, M. K. Sadan, M. Jeon, Gyu-Bong Cho, T.-H. Nam, K.-K. Cho, J.-H. Ahn, H.-J. Ahn, *J. Alloy. Compd.*, 2021, *886*, 161240.

2. X. Zhong, J. Duan, Y. Xiang, X. Hu, Y. Huang, Y. Li, W. Deng, G. Zou, H. Hou, X. Ji, *Adv. Funct. Mater.*, 2023, *33*, 2306574.

3. J. Yang, X. Guo, H. Gao, T. Wang, Z. Liu, Q. Yang, H. Yao, J. Li, C. Wang, G. Wang, *Adv. Energy Mater.*, 2023, *13*, 2300351.

4. F. Zhang, X. Liu, B. Wang, G. Wang, H. Wang, *ACS Appl. Mater. Interfaces*, 2021, *13*, 59867.

5. B. Pu, Y. Liu, J. Bai, X. Chu, X. Zhou, Y. Qing, Y. Wang, M. Zhang, Q. Ma, Z. Xu, B. Zhou, W. Yang, *ACS Nano*, 2022, *16*, 18746.

6. X. Li, S. Xiao, X. Niu, J. S. Chen, Y. Yu, *Adv. Funct. Mater.*, 2021, *31*, 2104798.

7. Y. Zhu, Q. Yao, R. Shao, C. Wang, W. Yan, J. Ma, D. Liu, Jian Yang, Y. Qian, *Nano Lett.*, 2022, *22*, 7976.

8. X. Hou, Y. Zhu, Q. Yao, J. Song, C. Wang, Y. Zhou, S. Zeng, J. Yang, Y. Qian, *J. Energy Chem.*, 2023, *79*, 468.

9. W. Zhang, W. Yan, H. Jiang, C. Wang, Y. Zhou, F. Ke, H. Cong, H. Deng, *ACS Sustainable Chem. Eng.*, 2019, *8*, 335.

10. Z. Chen, X. Wu, Z. Sun, J. Pan, J. Han, Y. Wang, H. Liu, Y. Shen, J. Li, D. Peng, Q. Zhang, *Adv. Energy Mater.*, 2024, *14*, 2400132.

11. H. Gao, J. Niu, C. Zhang, Z. Peng, Z. Zhang, *ACS Nano*, 2018, *12*, 3568.

12. Y. Zhu, X. Han, Y. Xu, Y. Liu, S. Zheng, K. Xu, L. Hu, C. Wang, *ACS Nano*, 2013, *7*, 76378.

13. W. He, K. Chen, R. Pathak, M. Hummel, K.M. Reza, N. Ghimire, J. Pokharel, S. Lu, Z. Gu, Q. Qiao, Y. Zhou, *Chem. Eng. J.*, 2021, *414*, 128638.